Directly Measuring the Degree of Quantum Coherence using Interference Fringes

Yi-Tao Wang, Jian-Shun Tang,* Zhi-Yuan Wei, Shang Yu, Zhi-Jin Ke, Xiao-Ye Xu, Chuan-Feng Li,† and Guang-Can Guo
CAS Key Laboratory of Quantum Information, University of Science and Technology of China, Hefei 230026, People's Republic of China
Synergetic Innovation Center of Quantum Information and Quantum Physics, University of Science and Technology of China, Hefei 230026, People's Republic of China
(Received 13 August 2016; revised manuscript received 17 November 2016; published 12 January 2017)

Quantum coherence is the most distinguished feature of quantum mechanics. It lies at the heart of the quantum-information technologies as the fundamental resource and is also related to other quantum resources, including entanglement. It plays a critical role in various fields, even in biology. Nevertheless, the rigorous and systematic resource-theoretic framework of coherence has just been developed recently, and several coherence measures are proposed. Experimentally, the usual method to measure coherence is to perform state tomography and use mathematical expressions. Here, we alternatively develop a method to measure coherence directly using its most essential behavior—the interference fringes. The ancilla states are mixed into the target state with various ratios, and the minimal ratio that makes the interference fringes of the "mixed state" vanish is taken as the quantity of coherence. We also use the witness observable to witness coherence, and the optimal witness constitutes another direct method to measure coherence. For comparison, we perform tomography and calculate l_1 norm of coherence, which coincides with the results of the other two methods in our situation. Our methods are explicit and robust, providing a nice alternative to the tomographic technique.

DOI: 10.1103/PhysRevLett.118.020403

Introduction.—Quantum coherence, also known as quantum superposition, is the most essential property that distinguishes quantum mechanics from classical theory. It is the fundamental resource for quantum information processing, such as quantum computation [1], quantum key distribution [2], and quantum metrology [3,4]. Other quantum resources, such as the asymmetry of quantum states, are proved to be related to the quantum coherence [5,6]; especially, the entanglement and other quantum correlations are even regarded as a special kind of quantum coherence in bi- and multipartite situations [7,8]. Moreover, the quantum coherence also plays an important role in the fields of superfluidity [9], thermodynamics [10–12], and quantum biology (e.g., the photosynthetic light harvesting) [13,14], etc. Although there has been a long history in the studies of quantum coherence in various systems [15–24], especially in quantum optics [15–18], the coherence was subjected to the rigorous and systematic resource-theoretic framework [25,26] just in recent years [27,28] (see Supplemental Material [29]). One of the primary contents of this resource-theoretic framework is the quantification of the quantum coherence, which should be restricted by the conditions of the resource theory [28,34]. After the seminal work of Baumgratz *et al.*, in which a class of coherence measures based on different state distances were proposed [28], many other types of coherence measures have been raised, for example, the measure based on the Wigner-Yanase-Dyson skew information [35], the measures based on entanglement [36], and the measure based on robustness [6,30], etc.

Practically, the often-used method to carry out the coherence measurement on a quantum system is to perform the state tomography [31,37] and then, subject the derived state density matrix to the expressions of the coherence measures. However, the whole measurement process is largely dependent on the mathematical calculations. The physical effect of the coherence, i.e., the interference, is actually not reflected very directly during the measurement process. Moreover, the state-tomography method may contain redundant information. When measuring the coherence of a quantum system, we actually do not need to know the full information about its state because not all the information about the this state is related to the quantity that we desire. Therefore, particular methods can be designed to directly measure the quantum coherence without tomography. Similar (but not the same) situations also appear in the measurement of other quantum resources, such as the detection of the quantum system-environment correlations using local operation [38–40] or some other purposes like state discrimination [41].

In this Letter, we introduce a method—inspired by the ancilla-assisted measurement methods [6,30,42–44] and as an alternative to the tomographic technique—to measure the magnitude of the quantum coherence directly using its most remarkable feature, i.e., the interference fringes, and the polarization state of the single photons is used as the example to illustrate this method. During the measurement process, a varying ancilla state (τ) is mixed into the target state (ρ) with a varying ratio (denoted as s and which will be discussed later), and then, the visibility on the reference

 © 2017 American Physical Society

bases of the "mixed state" is monitored. The smallest ratio making the interference disappear is taken as the coherence value of the target state, denoted as $\mathcal{C}$. This measurement result is actually the robustness of coherence (ROC), which is defined in Ref. [6,30] as

$$\mathcal{C} = \min_{\tau \in \mathcal{D}} \left\{ s \geq 0 | \frac{\rho + s\tau}{1+s} \in \mathcal{I} \right\}, \tag{1}$$

where $\mathcal{D}$ is the convex set of all the qubit states, and $\mathcal{I} \subset \mathcal{D}$ denotes the subset of the incoherent states. ROC has been proven to be a bona fide measure of coherence [6,30], which satisfies all the conditions raised by the resource theory [28,34]. We also use the coherence-witness operators to detect the quantum coherence, and the result of the optimal coherence witness (denoted as $\mathcal{C}_{\mathcal{W}}$) becomes the same as the above-mentioned measurement result $\mathcal{C}$ (i.e., ROC), which provides another way to directly measure the quantum coherence, i.e., by using an observable [6,30]. Moreover, for the purpose of comparison, we still perform the state tomography for this instantiated situation and calculate the l_1 norm of coherence [defined as $\mathcal{C}_{l_1}(\rho) = \sum_{i,j,i\neq j} |\rho_{ij}|$]—a typical distance-based coherence measure (the l_1 norm distance between ρ and its corresponding incoherent state) [28]. Our results show that the values of the quantum coherence measured directly, using either the interference fringes or the optimal witness observable, are both the same as that of the l_1 norm of coherence, obtained by tomography in our instantiated situation [6,30], which shows the validity of our direct measurement methods.

The interference-fringe method.—The experimental setup is shown in Fig. 1, and details can be referred to in the Supplemental Material [29]. The target quantum state to be measured in our experiment is prepared in process (a). This state can be expressed as $\rho = \frac{1}{2}[\mathbb{1} + r_\rho(\sin\theta_\rho \cos\varphi_\rho \sigma_x + \sin\theta_\rho \sin\varphi_\rho \sigma_y + \cos\theta_\rho \sigma_z)]$, where $\mathbb{1}$ is the identity matrix, σ_x, σ_y, and σ_z are the Pauli matrices, θ_ρ and φ_ρ are the azimuth angles, and r_ρ is the radius of the state in the Bloch sphere. After the preparation, this state is sent to process (b) for the coherence measurement. As mentioned previously, during this process, an ancilla state is prepared, which can be expressed as $\tau = \frac{1}{2}[\mathbb{1} + r_\tau(\sin\theta_\tau \cos\varphi_\tau \sigma_x + \sin\theta_\tau \sin\varphi_\tau \sigma_y + \cos\theta_\tau \sigma_z)]$, with the symbols similar to those in ρ; especially, we denote $\Theta_\tau = \arccos(r_\tau \cos\theta_\tau)$ and $u_\tau = r_\tau \sin\theta_\tau$ [representing the distance between τ and r_z in the Bloch sphere; see Fig. 2(e)]. According to the definition Eq. (1), this ancilla state is mixed into the target state with a varying ratio s, and the state after mixing is $\mu = (\rho + s\tau)/(1+s)$. To check whether μ (s dependent) is in the incoherent-state set $\mathcal{I}$, the interference fringes of μ is monitored by detecting the probability of μ to collapse on the basis of $|f> = (|H\rangle + e^{i\phi}|V\rangle)/\sqrt{2}$, where $|H\rangle$ and $|V\rangle$ denote the horizontal- and vertical-polarization reference bases, respectively, and ϕ is the relative phase. The vanished visibility means $\mu \in \mathcal{I}$. Then, the next step of this method is to seek the optimal ancilla state τ^*, which provides the minimal s, while keeping the visibility of the interference fringes of the "mixed state" (μ) vanished. This minimal s value is just the coherence measure $\mathcal{C}$, according to the definition Eq. (1).

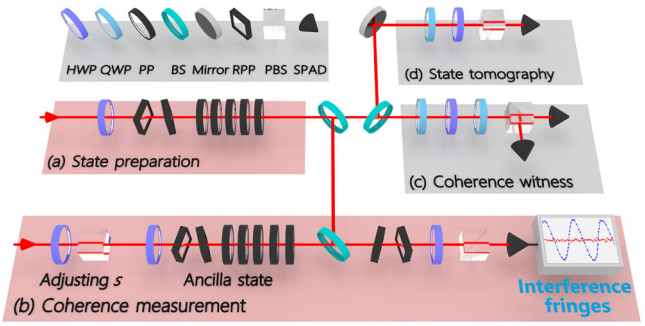

FIG. 1. Experimental setup. (a) The preparation of the target state. (b) The direct coherence-measurement method using the interference fringes. The same setups as those in (a) prepare the various ancilla states and the half-wave plate (HWP) and polarizing beam splitter (PBS) before it adjusts the mixing ratio s by tuning the number of the ancilla photons. Then, the beam splitters (BSs) mix the target and ancilla states. The following rotated phase plates (RPPs), HWP, PBS, and the electronic module detect and monitor the interference fringes. The inset figure on the top of the box are actually two sample fringe data that we obtain. The blue and red dots, respectively, correspond to the "mixed state" with and without coherence. (c) The method using coherence-witness observable. The quarter-wave plates (QWPs) and HWP can map the bases of the PBS to the eigenstates of any witness observable. Each of the eigenstates corresponds to the detection events with the value of the corresponding eigenvalue. Then, the expectation value of the events can be calculated. (d) Tomography method. Details can be referred to in Ref. [31] and Supplemental Material [29]. PP, phase plate; SPAD, single-photon avalanche diode.

The searching process for τ^* can be various, for example, the traversal method and the Bayesian method [45], etc. To show the characteristics of the monitored interference fringes more completely and clearly, we adopt the traversal method. However, we emphasize that this searching process can be more efficient when other methods are utilized; especially, in some particular situations, the full searching process can be greatly simplified; e.g., in our situation, the ancilla state contains three parameters to be scanned for a full search, i.e., φ_τ, u_τ, and θ_τ, but we will show that later, the u_τ and θ_τ scannings are trivial for a qubit system, and only φ_τ scanning is necessary. Here, the ρ state with $r_\rho = 0.97$, $\theta_\rho = 63°$, and $\varphi_\rho = 0°$, is taken as the example to illustrate the full search process. The first step is to sweep the parameter φ_τ, and the visibility results (denoted as V) are shown in Figs. 2(a) and 2(b); (b) is the enlargement of the red dashed rectangle in (a), using different dots, with the lines being the corresponding theoretical simulations (the

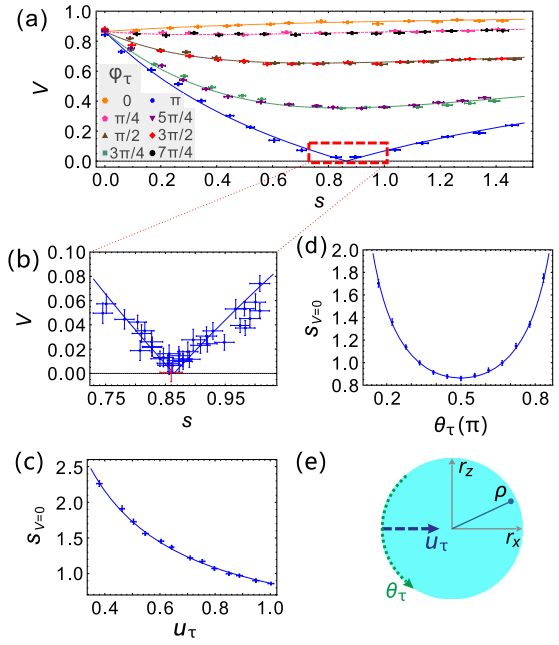

FIG. 2. Searching process for τ^* (part of the interference-fringe method). (a) The typical results of sweeping φ_τ ($\varphi_\tau = n\pi/4$, with $n = 0$ to 7). V is the visibility of the interference fringes of the "mixed state," and the mixing ratio s is determined by the finally detected photon numbers of, respectively, the target and ancilla states. The dots are the experimental data, and the lines are the corresponding theoretical simulations. The error bars originate from the fitting errors of the interference fringes. (b) The enlargement of the red dashed rectangle in (a). The minimum visibility is marked using red color, and it vanishes within the error bar. The corresponding s is denoted as $s_{V=0}$, which only appears when $\varphi_\tau = \varphi_\rho + \pi$. (c) The typical results of sweeping u_τ [along the blue dashed arrow in (e)]. The minimum $s_{V=0}$ appears when $u_\tau = \sin\theta_\tau$ (or $r_\tau = 1$), i.e., the pure state situation. (d) The typical results of sweeping θ_τ [along the green dotted arrow in (e)]. The minimum $s_{V=0}$ appears when $\theta_\tau = \pi/2$. (e) The cross section of the Bloch sphere in the $r_x - r_z$ plane.

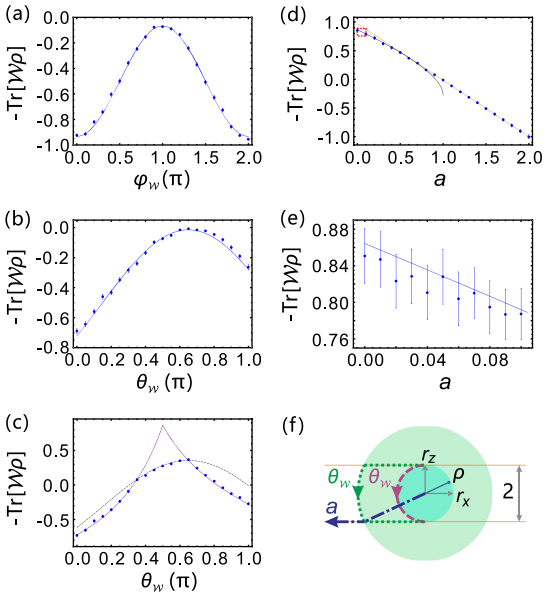

FIG. 3. Searching process for $\mathcal{W}^*$ (part of the witness-observable method). (a) The typical results of sweeping $\varphi_\mathcal{W}$. The dots are experimental data, and the line is the theoretical simulation. The error bars originate from the standard deviation. The maximum $-\mathrm{Tr}[\rho\mathcal{W}]$ appears when $\varphi_\mathcal{W} = \varphi_\rho + \pi$. (b) The typical results of sweeping $\theta_\mathcal{W}$ in the $0 \le r_\mathcal{W} \le 1$ case [along the purple dashed arrow in (f)]. The maximum $-\mathrm{Tr}[\rho\mathcal{W}]$ appears when $\theta_\mathcal{W} = \pi - \theta_\rho$. (c) The typical results of sweeping $\theta_\mathcal{W}$ in the $r_\mathcal{W} > 1$ case [along the green dotted arrow in (f)]. The maximum $-\mathrm{Tr}[\rho\mathcal{W}]$ appears between $\pi - \theta_\rho$ and $\pi/2$. All the maximums of (b),(c) are marked in (f) using the blue dot-dashed arrow. (d) The results of sweeping $r_\mathcal{W} = 2/a - 1$ (a) along the blue dot-dashed arrow. (e) The enlargement of the red dashed rectangle in (d). The maximum $-\mathrm{Tr}[\rho\mathcal{W}]$ appears when $a = 0$, i.e., $\mathcal{W}^* = -(\cos\varphi_\rho\sigma_x + \sin\varphi_\rho\sigma_y)$. (f) The cross section of the $\mathcal{W}$'s space in the $r_x - r_z$ plane. All possible $\mathcal{W}$'s are sandwiched between the planes of $r_z = \pm 1$.

same below in Fig. 2 and Fig. 3). We should note that here, only the typical data are shown in Fig. 2 and Fig. 3, and other corresponding data are similar. The detailed parameters of the showed data can be referred to in the captions of these figures. These φ_τ-sweeping results indicate that only when $\varphi_\tau = \varphi_\rho + \pi$, the interference fringes of μ can disappear; especially, see the visibility data marked using red dot in Fig. 2(b), which reaches zero within its error bar. Therefore, φ_τ is set as $\varphi_\rho + \pi$ in the following steps, and the incoherent μ (i.e., μ with $V = 0$) can always be obtained with a proper s (denoted as $s_{V=0}$). The second step is to sweep the parameter u_τ for each fixed Θ_τ along the direction shown in Fig. 2(e) (the cross section of the Bloch sphere in the $r_x - r_z$ plane), using the blue dashed arrow, and the results are shown in Fig. 2(c). It is clear that the minimal $s_{V=0}$ to derive the incoherent μ is obtained when the condition $u_\tau = \sin\theta_\tau$ is fulfilled, i.e., $r_\tau = 1$, the pure state situation. The last step is then to sweep the parameter θ_τ in the pure states along the direction represented by the green dotted arrow. Figure 2(d) shows the results, which indicate that the minimal $s_{V=0}$ is obtained when $\theta_\tau = \pi/2$. Therefore, after these sweeping steps, we derive the optimal ancilla state to be the state satisfying $r_{\tau^*} = 1$, $\theta_{\tau^*} = \pi/2$, and $\varphi_{\tau^*} = \varphi_\rho + \pi$ [i.e., $|\psi_{\tau^*}\rangle = (1/\sqrt{2})(|H\rangle - e^{i\varphi_\rho}|V\rangle)$ or $1/\sqrt{2}(|H\rangle - |V\rangle)$ for this $\varphi_\rho = 0$ case], and the mixing ratio s, making μ incoherent in this case, is the measured coherence of the target state ρ, which is $\mathcal{C} = 0.860 \pm 0.019$. We find that u_{τ^*} (r_{τ^*}) and θ_{τ^*} are independent of the target state ρ, which means the scannings for the corresponding parameters are trivial, so the number of the searching parameters for τ^* can be reduced to 1; the full process can be simplified.

The witness-observable method.—The target state is also sent to the process shown in Fig. 1(c) for the coherence witness. During this process, the expectation value of a witness observable $\mathcal{W}$ is detected under the target state of the single photons (details on the experimental descriptions and the data analysis are seen in the Supplemental Material

[29]). The witness observable $\mathcal{W}$ has the following properties [6,30]: (1) $\mathrm{Tr}[\rho\mathcal{W}] \geq 0$ for all incoherent states, which means once the negative expectation value emerges, we can conclude the target state contains the coherence; (2) $-\mathrm{Tr}[\rho\mathcal{W}] \leq \mathcal{C}$ always holds for all possible $\mathcal{W}$, and there always exists an optimal $\mathcal{W}$ (denoted as $\mathcal{W}^*$), which makes the equation reached, which means another way to directly measure the coherence of ρ, i.e., the observable method, and this coherence measure can be written as $\mathcal{C}_\mathcal{W} := -\mathrm{Tr}[\rho\mathcal{W}^*]$. $\mathcal{W}$ can be expressed as $\mathcal{W} = (a/2)[\mathbb{1} + r_\mathcal{W}(\sin\theta_\mathcal{W}\cos\varphi_\mathcal{W}\sigma_x + \sin\theta_\mathcal{W}\sin\varphi_\mathcal{W}\sigma_y + \cos\theta_\mathcal{W}\sigma_z)]$, which has also some constraint conditions: $0 \leq a$ (real) ≤ 2, $r_\mathcal{W} \leq 2/a - 1$, and $-1 \leq r_\mathcal{W}\cos\theta_\mathcal{W} \leq 1$ (these conditions can be clearly illustrated in Fig. 3(f), and details on the derivation of these conditions can be found in Ref. [6] and the Supplemental Material [29]). In other words, all possible $\mathcal{W}$'s are sandwiched between the planes of $r_z = \pm 1$ in the $\mathcal{W}$'s space [corresponding to the space of Bloch sphere, see Fig. 3(f)]. Similar to the interference-fringe method, the next step of this observable method is to seek the optimal witness operator $\mathcal{W}^*$ and furthermore, detect $\mathcal{C}_\mathcal{W}$.

Similar to the searching process for τ^*, we also adopt the traversal searching method for $\mathcal{W}^*$ for the purpose of completeness. As discussed above, the searching parameters here are $\varphi_\mathcal{W}$, $\theta_\mathcal{W}$, and $r_\mathcal{W}$ (or a), respectively. The first step is to sweep the parameter $\varphi_\mathcal{W}$, and the typical data can be seen in Fig. 3(a). When $\varphi_\mathcal{W} = \varphi_\rho + \pi$, $-\mathrm{Tr}[\rho\mathcal{W}]$ reaches its maximum. The second step is to sweep the parameter $\theta_\mathcal{W}$. Figures 3(b) and 3(c) show the results obtained by sweeping $\theta_\mathcal{W}$ along the paths indicated, using the purple dashed arrow and the green dotted arrow shown in Fig. 3(f), respectively. Figure 3(f) is the cross section of the $\mathcal{W}$'s space in the $r_x - r_z$ plane. Figure 3(b) corresponds to the case of $0 \leq r_\mathcal{W} \leq 1$. The maximum $-\mathrm{Tr}[\rho\mathcal{W}]$ is obtained when $\theta_\mathcal{W} = \pi - \theta_\rho$ (i.e., 117°). Figure 3(c) corresponds to the case of $r_\mathcal{W} > 1$. The optimal $\theta_\mathcal{W}$ varies from $\pi - \theta_\rho$ to $\pi/2$ as the increasing of $r_\mathcal{W}$. All the optimal cases of both Figs. 3(b) and 3(c) are marked using the blue dot-dashed arrow in Fig. 3(f). By sweeping the parameter $r_\mathcal{W} = 2/a - 1$ (or a) along this path, we obtain the results shown in Figs. 3(d), 3(e), with the latter being the enlargement of the red dashed rectangle in the former figure. These results indicate that the value of $-\mathrm{Tr}[\rho\mathcal{W}]$ increases as the increasing of $r_\mathcal{W}$, i.e., the decreasing of a, and the optimal a is zero. Consequently, the optimal coherence-witness observable $\mathcal{W}^*$ should satisfy $\varphi_{\mathcal{W}^*} = \varphi_\rho + \pi$, $\theta_{\mathcal{W}^*} = \pi/2$, $a_{\mathcal{W}^*} = 0$, and $r_{\mathcal{W}^*} = 2/a_{\mathcal{W}^*} - 1$. In this case, although $r_{\mathcal{W}^*}$ does not converge, $\mathcal{W}^*$ is convergent, which is $\mathcal{W}^* = -(\cos\varphi_\rho\sigma_x + \sin\varphi_\rho\sigma_y)$ ($-\sigma_x$ for this $\varphi_\rho = 0$ case). We want to note that, during this method, we always set $r_\mathcal{W} = 2/a - 1$ because $-\mathrm{Tr}[\rho\mathcal{W}]$ for the $r_\mathcal{W} < 2/a - 1$ case is always less than that of the $r_\mathcal{W} = 2/a - 1$ case. The result of the optimal witness of the coherence is $\mathcal{C}_\mathcal{W} = 0.851 \pm 0.030$. In this particular situation, we can find that the scannings for $\theta_\mathcal{W}$ and $r_\mathcal{W}$ (or a) are trivial because θ_{W^*}, $a_{\mathcal{W}^*}$, and r_{W^*} are independent of ρ, and the only parameter that needs to be scanned is $\varphi_\mathcal{W}$, which means this searching process can be greatly simplified.

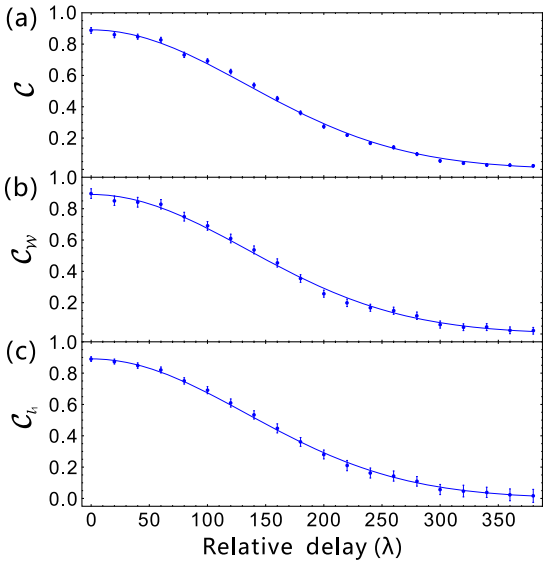

FIG. 4. Results of the three coherence-measurement methods ($\mathcal{C}$, $\mathcal{C}_\mathcal{W}$, and $\mathcal{C}_{l_1}$ that are shown in (a), (b), and (c), respectively). The target state is varied by going through a pure-dephasing evolution. The lines are the corresponding theoretical fits for these data.

Comparison of the results of the three coherence-measurement methods.—For the purpose of comparison, we send the same target state ρ to the tomography process shown in Fig. 1(d), which generally bases on the maximum-likelihood-estimation method (details on the tomography process can be found in Ref. [31] and the Supplemental Material [29]). We then calculate the l_1 norm of coherence through the derived density matrix and obtain $\mathcal{C}_{l_1} = 0.874 \pm 0.015$. This value is almost the same as those of $\mathcal{C}$ and $\mathcal{C}_\mathcal{W}$ for this instantiated ρ. Moreover, we prepare a series of target states with a pure state going through a pure-dephasing channel (a pure-dephasing dynamical evolution). The channel length is proportional to the relative delay between the two eigenmodes of the channel and is varied by inserting different numbers of the phase plates (PPs) in Fig. 1(a). The instantiated ρ discussed above corresponds to the state with the relative delay of 20λ. All the results of $\mathcal{C}$, $\mathcal{C}_\mathcal{W}$, and $\mathcal{C}_{l_1}$ are shown in Fig. 4(a), 4(b), and 4(c), respectively, and the lines are the corresponding fits. These three results coincide with each other well and they all show the decay of coherence as the channel length increases. Actually, it has been proved theoretically that all these three quantities are equivalent for the qubit system [6,30]. The experimental results shown in Fig. 4 validate the reliability of our methods to directly measure the coherence of the target state, using the interference fringes and the optimal witness observable.

Conclusions.—We have developed the methods to directly measure the quantum coherence, using the interference

fringes and the optimal witness observable, and compare their results with l_1 norm of coherence. These three results coincide with each other for our polarization states. The interference-fringe method is explicit in the physical meanings and robust for various sources of ancilla state [according to Eq. (1)]. The witness-observable method is direct in a way of observable measurement. Moreover, both our methods and the tomography method contain the searching processes. The difference is that our searching processes are based on the experimental detections and that tomography relies on the likelihood-function calculation (details about these discussions can be found in the Supplemental Material [29]), but this point becomes more and more trivial when all the parameter controls and the data acquisitions are integrated into one single computer program. Therefore, our methods provide a nice alternative to the state tomography method.

We are grateful to G. Adesso for valuable discussions. This work is supported by the National Natural Science Foundation of China (Grants No. 61490711, No. 11674304, No. 11474267, No. 11274289, No. 11304305, No. 11325419, No. 61327901, and No. 91321313), the Strategic Priority Research Program(B) of the Chinese Academy of Sciences (Grant No. XDB01030300), the Key Research Program of Frontier Sciences of the Chinese Academy of Sciences (Grant No. QYZDY-SSW-SLH003). C.-F. L. acknowledges support from the EU Collaborative project QuProCS (641277).

*tjs@ustc.edu.cn
†cfli@ustc.edu.cn

[1] M. A. Nielsen and I. L. Chuang, *Quantum Computation and Quantum Information* (Cambridge University Press, Cambridge, UK, 2000).
[2] N. Gisin, G. Ribordy, W. Tittel, and H. Zbinden, Rev. Mod. Phys. **74**, 145 (2002).
[3] V. Giovannetti, S. Lloyd, and L. Maccone, Science **306**, 1330 (2004).
[4] V. Giovannetti, S. Lloyd, and L. Maccone, Nat. Photonics **5**, 222 (2011).
[5] I. Marvian and R. W. Spekkens, Nat. Commun. **5**, 3821 (2014).
[6] M. Piani, M. Cianciaruso, T. R. Tromley, C. Napoli, N. Johnston, and G. Adesso, Phys. Rev. A **93**, 042107 (2016).
[7] C. Radhakrishnan, M. Parthasarathy, S. Jambulingam, and T. Byrnes, Phys. Rev. Lett. **116**, 150504 (2016).
[8] K. C. Tan, H. Kwon, C.-Y. Park, and H. Jeong, Phys. Rev. A **94**, 022329 (2016).
[9] O. Penrose and L. Onsager, Phys. Rev. **104**, 576 (1956).
[10] M. Lostaglio, D. Jennings, and T. Rudolph, Nat. Commun. **6**, 6383 (2015).
[11] M. Lostaglio, K. Korzekwa, D. Jennings, and T. Rudolph, Phys. Rev. X **5**, 021001 (2015).
[12] V. Narasimhachar and G. Gour, Nat. Commun. **6**, 7689 (2015).
[13] N. Lambert, Y.-N. Chen, Y.-C. Cheng, C.-M. Li, G.-Y. Chen, and F. Nori, Nat. Phys. **9**, 10 (2013).
[14] S. F. Huelga and M. B. Plenio, Nat. Phys. **10**, 621 (2014).
[15] R. J. Glauber, Phys. Rev. **131**, 2766 (1963).
[16] E. C. G. Sudarshan, Phys. Rev. Lett. **10**, 277 (1963).
[17] L. Mandel and E. Wolf, *Optical Coherence and Quantum Optics* (Cambridge University Press, Cambridge, England, 1995).
[18] K. H. Kagalwala, G. D. Giuseppe, A. F. Abouraddy, and B. E. A. Saleh, Nat. Photonics **7**, 72 (2013).
[19] A. Yacoby, M. Heiblum, D. Mahalu, and H. Shtrikman, Phys. Rev. Lett. **74**, 4047 (1995).
[20] I. Chiorescu, Y. Nakamura, C. J. P. M. Harmans, and J. E. Mooij, Science **299**, 1869 (2003).
[21] U. L. Andersen, M. Sabuncu, R. Filip, and G. Leuchs, Phys. Rev. Lett. **96**, 020409 (2006).
[22] M. Sabuncu, L. Mista, J. Fiurasek, R. Filip, G. Leuchs, and U. L. Andersen, Phys. Rev. A **76**, 032309 (2007).
[23] M. Lassen, M. Sabuncu, A. Huck, J. Niset, G. Leuchs, N. J. Cerf, and U. L. Andersen, Nat. Photonics **4**, 700 (2010).
[24] C. Li, N. Lambert, Y. Chen, G. Chen, and F. Nori, Sci. Rep. **2**, 885 (2012).
[25] I. Devetak, A. W. Harrow, and A. J. Winter, IEEE Trans. Inf. Theory **54**, 4587 (2008).
[26] M. Horodecki and J. Oppenheim, Int. J. Mod. Phys. B **27**, 1345019 (2013).
[27] J. Åberg, arXiv:quant-ph/0612146.
[28] T. Baumgratz, M. Cramer, and M. B. Plenio, Phys. Rev. Lett. **113**, 140401 (2014).
[29] See Supplemental Material at http://link.aps.org/supplemental/10.1103/PhysRevLett.118.020403, which includes Refs. [6,28,30–33], for the experimental details and discussion.
[30] C. Napoli, T. R. Bromley, M. Cianciaruso, M. Piani, N. Johnston, and G. Adesso, Phys. Rev. Lett. **116**, 150502 (2016).
[31] D. F. V. James, P. G. Kwiat, W. J. Munro, and A. G. White, Phys. Rev. A **64**, 052312 (2001).
[32] J. Eisert, F. G. S. L. Brandão, and K. M. R. Audenaert, New J. Phys. **9**, 46 (2007).
[33] R. Horodecki, P. Horodecki, M. Horodecki, and K. Horodecki, Rev. Mod. Phys. **81**, 865 (2009).
[34] T. R. Bromley, M. Cianciaruso, and G. Adesso, Phys. Rev. Lett. **114**, 210401 (2015).
[35] D. Girolami, Phys. Rev. Lett. **113**, 170401 (2014).
[36] A. Streltsov, U. Singh, H. S. Dhar, M. N. Bera, and G. Adesso, Phys. Rev. Lett. **115**, 020403 (2015).
[37] A. I. Lvovsky and M. G. Raymer, Rev. Mod. Phys. **81**, 299 (2009).
[38] M. Gessner and H.-P. Breuer, Phys. Rev. Lett. **107**, 180402 (2011).
[39] M. Gessner, M. Ramm, T. Pruttivarasin, A. Buchleitner, H-P. Breuer, and H. Häffner, Nat. Phys. **10**, 105 (2014).
[40] J.-S. Tang *et al.*, Optica **2**, 1014 (2015).
[41] J. Niset, A. Acín, U. L. Andersen, N. J. Cerf, R. García-Patrón, M. Navascués, and M. Sabuncu, Phys. Rev. Lett. **98**, 260404 (2007).
[42] R. S. Bennink, S. J. Bentley, and R. W. Boyd, Phys. Rev. Lett. **89**, 113601 (2002).
[43] J. B. Altepeter, D. Branning, E. Jeffrey, T. C. Wei, P. G. Kwiat, R. T. Thew, J. L. O'Brien, M. A. Nielsen, and A. G. White, Phys. Rev. Lett. **90**, 193601 (2003).
[44] M. Sabuncu, R. Filip, G. Leuchs, and U. L. Andersen, Phys. Rev. A **81**, 012325 (2010).
[45] D. S. Sivia and J. Skilling, *Data Analysis: A Bayesian Tutorial*, 2nd ed. (Oxford University Press, Oxford, 2006).